Mechanism and Dynamics of Interligand Electron Transfer in *fac*-[Re(MQ$^+$)(CO)$_3$(dmb)]$^{2+}$. An Ultrafast Time-Resolved Visible and IR Absorption, Resonance Raman, and Emission Study (dmb = 4,4′-Dimethyl-2,2′-bipyridine, MQ$^+$ = *N*-Methyl-4,4′-bipyridinium)

Davina J. Liard,[†] Michael Busby,[†] Ian R. Farrell,[†] Pavel Matousek,[‡] Michael Towrie,[‡] and Antonín Vlček, Jr.*,[†]

Department of Chemistry and Centre for Materials Research, Queen Mary, University of London, Mile End Road, London E1 4NS, United Kingdom, and Central Laser Facility, CCLRC Rutherford Appleton Laboratory, Chilton, Didcot, Oxfordshire OX11 0QX, United Kingdom

Received: September 20, 2003; In Final Form: November 12, 2003

A comprehensive understanding of ultrafast excited-state dynamics of *fac*-[Re(MQ$^+$)(CO)$_3$(dmb)]$^{2+}$ (MQ$^+$ = *N*-methyl-4,4′-bipyridinium, dmb = 4,4′-dimethyl-2,2′-bipyridine) was achieved by combining several time-resolved investigations: visible and IR absorption, resonance Raman, and emission. Optical excitation of *fac*-[Re(MQ$^+$)(CO)$_3$(dmb)]$^{2+}$ populates a Re → dmb ^{3}MLCT (MLCT = metal-to-ligand charge transfer) excited state which undergoes dmb$^{\bullet-}$ → MQ$^+$ interligand electron transfer (ILET) to form a Re → MQ$^+$ ^{3}MLCT excited-state *fac*-^{3}[Re^{II}(MQ$^\bullet$)(CO)$_3$(dmb)]$^{2+}$. ILET rates were measured in a series of solvents by time-resolved visible absorption spectroscopy. Time constants range from 8 to 18 ps. Picosecond time-resolved resonance Raman and IR spectroscopies have revealed that ILET is accompanied by a large structural reorganization of the MQ and Re(CO)$_3$ moieties. The MQ$^\bullet$ ligand attains a quinoidal structure while positive shifts of ν(CO) absorption bands indicate shortening of C≡O bonds due to a decrease of electron density on Re upon ILET. Hence, a relatively large reorganization energy is implicated. Both Raman and IR bands undergo a solvent-dependent dynamic blue shift and narrowing on a picosecond time scale, showing that the ILET product *fac*-^{3}[Re^{II}(MQ$^\bullet$)(CO)$_3$(dmb)]$^{2+}$ is initially formed "hot"—highly excited in low-frequency modes that are anharmonically coupled to the intra-MQ$^\bullet$ and ν(CO) vibrations. Moreover, it is shown that the Re → dmb ^{3}MLCT precursor state remains vibrationally excited on a time scale comparable with that of ILET. Three kinds of convoluted vibrational dynamics related to ILET are thus indicated: (i) cooling of the precursor state alongside ILET, (ii) an "instantaneous" change in the frequencies of high-frequency vibrations upon ILET, and (iii) cooling of the ILET product. The ILET rate does not correlate with any relevant solvent property (solvent function, relaxation time, LUMO energy, ionization potential). Apparently, the only way the solvent affects the ILET rate is through changing the driving force. ILET is much faster than expected from conventional electron-transfer theories. Analysis in terms of Marcus and Jortner−Bixon theories shows that the electronic coupling through the Re atom is relatively large, ≥130 cm^{-1}, making ILET (partly) adiabatic. Its unexpectedly fast rate is attributed to a strong involvement of intramolecular vibrational modes of the precursor state.

Introduction

Photoinduced intramolecular electron transfer attracts much research interest because of its fundamental importance and relevance to light−energy conversion and molecular electronics.[1−4] Both these potential areas of application rely on rapid and efficient formation of charge-separated states by very fast electron transfer that is competitive with energy-degrading processes. In general, the rate of nonadiabatic electron transfer between a covalently bridged electron donor and acceptor can be controlled by the chemical nature of the bridging group and dielectric properties of the solvent, which determine electronic coupling and outer-sphere reorganization energy, respectively.[3,5−7] Moreover, conformational dynamics could also be important, since the electronic coupling depends on the relative orientation of the donor, acceptor, and bridging moieties. Intramolecular vibrations and solvent relaxation dynamics become important if the electronic coupling is large, making the reaction at least partly adiabatic. It appears that adiabaticity can be important even in the case of a long-range electron transfer. For example, the surprising near independence of the electron-transfer rate of the length of oligophenylenevinylene molecular wires has been tentatively explained by an adiabatic mechanism.[8]

Most of the electron-transfer dyads studied so far undergo nonadiabatic electron transfer through an organic group that bridges between the electron donor and acceptor. A very interesting situation arises if the donor and acceptor are two different ligands in the coordination sphere of the same metal atom. Intramolecular electron transfer between such sites is then called *interligand electron transfer*, ILET. It occurs, for example, between bipyridine ligands in ^{3}MLCT (MLCT = metal-to-ligand charge transfer) excited states of bis- or trisbipyridine complexes such as [M(bpy)$_3$]$^{2+}$ (M = Ru, Os)[9−11] or [Ru(bpy-4,4′-(COOH)$_2$)$_2$(NCS)$_2$].[12] The excited electron is localized at a single bpy$^{\bullet-}$ ligand, and interligand electron transfer bpy$^{\bullet-}$ → bpy occurs on a picosecond time scale without a net change in

[†] University of London.
[‡] CCLRC Rutherford Appleton Laboratory.

10.1021/jp036822a CCC: $27.50
Published on Web 01/06/2004

SCHEME 1: Excited-State Behavior of *fac*-[Re(MQ$^+$)(CO)$_3$(dmb)]$^{2+}$ and Schematic Structures of the Species Involved[a]

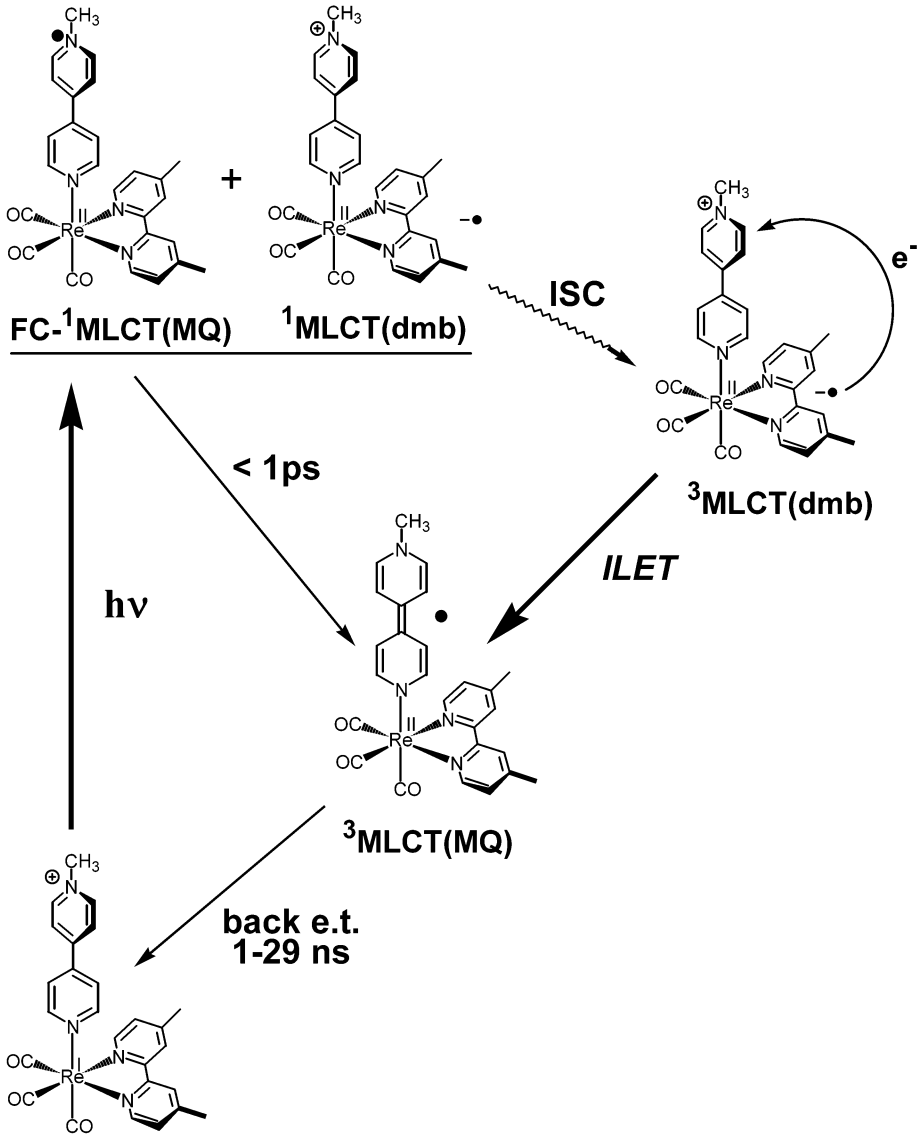

[a] FC-^{1}MLCT(MQ) stands for the optically populated (Franck−Condon) ^{1}MLCT(MQ) excited state which undergoes a rapid relaxation to the ^{3}MLCT(MQ) state. All the Re complexes discussed herein are of *facial* geometry, as shown. The *fac* prefix will be omitted hereinafter.

free energy. Similar, albeit slower, ILET takes place in ground states of reduced polypyridine complexes [M(bpy$^{\bullet-}$)(bpy)$_2$]$^+$ (M = Ru or Fe),[13] as well as in ground and excited states of dioxolene complexes which contain catecholate and semiquinone ligands.[14−17] ILET is pertinent also to ^{3}MLCT excited states of complexes containing chemically different acceptor ligands such as [Os(bpy)$_2$(mab)]$^{2+}$ (mab = monoamide functionalized bpy),[11] [Ru(phen)$_2$(dppz)]$^{2+}$ (dppz = dipyridophenazine),[18] or *fac*-[Re(MQ$^+$)(CO)$_3$(bpy)]$^{2+}$ (MQ$^+$ = *N*-methyl-4,4′-bipyridinium).[19−23] The ILET dynamics are closely related to the long-standing question of electron localization in ^{3}MLCT excited states of polypyridyl complexes[9−11,24,25] and link conceptually electron transfer with nonradiative internal conversion between excited states. From a more practical point of view, ILET can interfere with other excited-state reactions, in particular with electron or energy transfer to external acceptors.[12] One may also envisage that ILET can be used in molecular devices to route the excited electron from a chromophoric group to other parts of the molecule or molecular assembly.

The ILET mechanism and the factors which determine its rate are still only little understood. For example, ultrafast time-resolved spectroscopic measurements on [Os(bpy)$_3$]$^{2+}$ have led to somewhat conflicting results.[10,11] The latest study has found a time constant of 8.7 ps and proposed that the reaction is partly adiabatic, depending on the solvent.[11] A 700 fs ILET time was determined for the "luminescence switch" [Ru(phen)$_2$(dppz)]$^{2+}$ in an aqueous solution, which extends to 7 ps upon intercalation into DNA.[18] ILET represents a fascinating and little explored area of electron-transfer reactivity which offers an opportunity to study electronic coupling through metal atoms in different oxidation states, adiabatic effects, and relationships between solvation and electron-transfer dynamics and to develop new functional units for molecular devices.

fac-[Re(MQ$^+$)(CO)$_3$(dmb)]$^{2+}$ (dmb = 4,4′-dimethyl-2,2′-bipyridine) is a prototypical example of a metal-bridged electron-transfer dyad in which ILET occurs with a considerable driving force; see Scheme 1.[19−23] Optical excitation at 400 nm or in the near-UV spectral region populates simultaneously Re → dmb and Re → MQ$^+$ metal-to-ligand charge-transfer excited states, in which an electron is excited from a predominantly Re d(π) orbital to a π^* orbital of the dmb or MQ$^+$ ligand, respectively. Hereinafter, these excited states will be abbreviated MLCT(dmb) and MLCT(MQ). The ^{3}MLCT(dmb) state, which can be approximately viewed as *fac*-[Re^{II}(MQ$^+$)(CO)$_3$(dmb$^{\bullet-}$)]$^{2+}$, un-

dergoes a $dmb^{\bullet-} \rightarrow MQ^+$ ILET which produces a relaxed MLCT(MQ) state, *fac*-$[Re^{II}(MQ^{\bullet})(CO)_3(dmb)]^{2+}$; see Scheme 1. The ^{3}MLCT(MQ) state then decays to the ground state by a back electron transfer with a time constant of 1.2−29 ns, depending on the solvent.[26] Transient visible absorption[20] and resonance Raman[22] spectra reveal that the $MQ^{\bullet}$ ligand in the ^{3}MLCT(MQ) state has a planar quinoidal structure (Scheme 1).

Recently, we have investigated the dynamics of the $dmb^{\bullet-} \rightarrow MQ^+$ ILET in *fac*-$[Re(MQ^+)(CO)_3(dmb)]^{2+}$ using femtosecond time-resolved absorption spectroscopy and found ILET times of 8.3 and 14 ps in CH_3CN and ethylene glycol, respectively.[23] This result was interpreted as evidence for a change of the electron-transfer regime from nonadiabatic to partly adiabatic upon changing the solvent from quickly relaxing CH_3CN to "slow" ethylene glycol.[23] However, this conclusion is rather tentative, being based on a comparison of only two solvents. In fact, the actual situation might be more complicated, since ILET could proceed via a through-space mechanism, involving tunneling through solvent molecules[27] inserted between the dmb and MQ^+ ligands. In this case, the electronic coupling would be solvent-dependent. To understand the solvent role in detail, we have studied the ILET dynamics of $[Re(MQ^+)(CO)_3(dmb)]^{2+}$ in various solvents having different relaxation times, as well as chemical nature. However, kinetic data alone cannot answer important mechanistic questions concerning the role of vibrational activation and structural reorganization in the ILET mechanism. With the aim to build up a comprehensive understanding of the ILET mechanism, we have measured solvent effects on the ILET rate while the structural changes of the MQ^+ ligand and the $Re(CO)_3$ unit upon ILET were investigated by picosecond time-resolved resonance Raman (TR^3) and IR absorption spectroscopy, respectively. The behavior of *fac*-$[Re(MQ^+)(CO)_3(dmb)]^{2+}$ is always compared with that of the reference complex *fac*-$[Re(Etpy)(CO)_3(dmb)]^+$, which contains a redox-inactive 4-ethylpyridine ligand instead of the electron-accepting MQ^+.

Experimental Section

The complexes *fac*-$[Re(MQ)(CO)_3(dmb)](PF_6)_2$ and *fac*-$[Re(Etpy)(CO)_3(dmb)](PF_6)$ were prepared as described previously.[23] All solvents were obtained from Aldrich, usually in spectroscopic quality. They were used without any further purification. Deoxygenation was not necessary in view of the sample stability and all the dynamics being much faster than oxygen diffusion. The thermal and photochemical stabilities of the sample solutions during time-resolved spectroscopic measurements were checked by the UV−vis and/or IR spectra taken before and after the experiment. The sample decomposition was found to be negligible in all cases. Besides the inherent high stability of these compounds, this was ensured by circulating a relatively large volume of sample solution (ca. 20 mL) through a thin spectroscopic cell where only a very small spot of ca. 200 μm diameter was irradiated by the pump laser. (Defocusing to an area of 200−300 μm was used to measure visible absorption spectra.) The sample flowed through a 1 mm fused silica cell for visible absorption, while 1 and 0.5 mm open jets were used for time-resolved IR spectroscopy (TRIR) and TR^3 or emission studies, respectively.

Time-resolved visible, IR, Kerr-gate resonance Raman, and Kerr-gate emission measurements were done using the equipment and procedures described in detail previously.[28−33] In short, the sample solution was excited (pumped) at 400 nm, using frequency-doubled pulses from a Ti:sapphire laser of ∼200 fs duration (fwhm) in the case of time-resolved visible and IR absorption spectroscopy, while pulses of 1−2 ps duration were used for Raman and emission studies. Pump pulse energies of ∼2 μJ were used for visible and IR spectra, while 4.4−4.8 μJ was used for Raman and emission studies. The Raman probe pulse energy was 6 μJ at 600 nm and 4.8 μJ at 400 nm. A white-light continuum was used as a probe in visible absorption studies. TRIR spectra were probed with IR (∼200 fs) pulses obtained by difference-frequency generation. The IR probe pulses cover a spectral range 150−200 cm^{-1} wide. Kerr-gate TR^3 spectra were probed in the visible region (600 nm) using an OPA output. Some experiments employed frequency-doubled Ti:sapphire laser 400 nm pulses both as pump and probe, while 350 pump or probe pulses were obtained by the sum frequency generation of the 622 nm OPA output and the laser fundamental (800 nm). The Kerr gate was used to remove all long-lived emission from the Raman signal. The optical Kerr gate, operated by 800 nm Ti:sapphire laser pulses, was opened for an interval of ca. 4 ps to allow the instantaneous Raman scattering to pass through the detecting system while cutting off the longer lived emission. The same system was used to obtain time-resolved Kerr-gate emission spectra. In this case, no probe pulses were used. The emission was detected during the 4 ps intervals while the Kerr gate was opened. The sampling at different time delays was achieved by changing the delay between the pump pulse and the Kerr-gate opening. The magic-angle and parallel relative orientations of the polarization directions of the pump and probe beams were used in the absorption (vis, IR) and Raman experiments, respectively. The spectral resolution of TRIR and TR^3 experiments is ca. 4−5 cm^{-1}. Positions of peak maxima in TRIR and TR^3 spectra are determined with high accuracy by Lorentzian fitting.

The ILET kinetics were evaluated from the time evolution of the ca. 630 nm absorption band at time delays longer than 1 ps after the excitation. Identical kinetics were found at several wavelengths within this band. The time-dependent absorbance shows a single-exponential rise, followed by a much slower small exponential decay due to the back-reaction, which occurs on the time scale of a few nanoseconds. The rising part of the absorbance−time profile was fitted to the equation $A_0 + A_1 \exp(-t/\tau)$, where τ is the ILET time constant. Fitting to the equation $A = A_0 + A_1 \exp(-t/\tau) - A_2 \exp(-t/\tau_b)$, which includes the back-reaction, was attempted using τ_b values determined[26] separately. It was found that inclusion of the back-reaction has virtually no effect on the kinetic fits of the ILET. (A very small effect was found in the case of methylformamide, DMF, and DMSO, where the back-reaction is very fast, between 1 and 2 ns.)

The TR^3 spectra were corrected for the Raman signal due to the solvent and the ground state by subtracting the spectra obtained at negative time delays (−50 and −20 ps) and by subtracting any weak residual background emission that passed through the Kerr gate. The Raman and IR bands were then fitted as Lorentzian peaks. This fitting procedure yielded for each peak the time-dependent position, width, and area. It should be noted that the Raman and IR bands do not fit a Gaussian shape. Microcal Origin 5.0 or the custom-made Raman fitting software developed at RAL was used for the fitting.

Cyclic voltammograms were recorded on a potentiostat, model 270/250, EG&G Instruments Inc., Princeton Applied Research. A home-built electrochemical cell was used with a three-electrode system: working electrode (0.5 mm^2 Pt, 0.5 cm^2 glassy carbon or dropping Hg), auxiliary electrode (Pt coil), and an Ag-coil pseudoreference electrode. All values were obtained at a scan rate of 100 mV/s with either 0.1 M Bu_4NPF_6

or 0.1 M $LiClO_4$ supporting electrolyte and a 1−2 mM concentration of the complex. All redox potentials are reported against that of the ferrocene/ferrocenium (Fc/Fc^+) redox couple, which was used as an internal standard. Detailed experimental conditions are specified in Table 1.

Steady-state resonance Raman spectra for both complexes were obtained from acetonitrile solutions using a Dilor XY spectrometer using the 514.5 nm line of a Spectra Physics 2016 Ar^+ laser.

Results

$[Re(MQ^+)(CO)_3(dmb)]^{2+}$ was excited at 400 nm, into the onset of its lowest absorption band. Two MLCT transitions are simultaneously excited (eq 1), one being directed into the dmb ligand and the other to MQ^+.[22,23] Hereinafter, the resulting excited states are called MLCT(dmb) and MLCT(MQ), respectively. They can be approximately described as $[Re^{II}(MQ^+)(CO)_3(dmb^{\bullet-})]^{2+}$ and $[Re^{II}(MQ^{\bullet})(CO)_3(dmb)]^{2+}$, respectively. The $dmb^{\bullet-} \rightarrow MQ^+$ ILET (eq 2)

$$[Re^{I}(MQ^+)(CO)_3(dmb)]^{2+} \xrightarrow{h\nu} {}^1[Re^{II}(MQ^+)(CO)_3(dmb^{\bullet-})]^{2+} + {}^1[Re^{II}(MQ^{\bullet})(CO)_3(dmb)]^{2+}$$
$$\text{}^1\text{MLCT(dmb)} \qquad \text{FC-}^1\text{MLCT(MQ)} \tag{1a}$$

$${}^1[Re^{II}(MQ^+)(CO)_3(dmb^{\bullet-})]^{2+} \xrightarrow{\text{ISC}} {}^3[Re^{II}(MQ^+)(CO)_3(dmb^{\bullet-})]^{2+} \tag{1b}$$
$$\text{}^1\text{MLCT(dmb)} \qquad \text{}^3\text{MLCT(dmb)}$$

$${}^1[Re^{II}(MQ^{\bullet})(CO)_3(dmb)]^{2+} \xrightarrow{\text{ISC, relaxation}} {}^3[Re^{II}(MQ^{\bullet})(CO)_3(dmb)]^{2+} \tag{1c}$$
$$\text{FC-}^1\text{MLCT(MQ)} \qquad \text{}^3\text{MLCT(MQ)}$$

$${}^3[Re^{II}(MQ^+)(CO)_3(dmb^{\bullet-})]^{2+} \xrightarrow{\text{ILET}} {}^3[Re^{II}(MQ^{\bullet})(CO)_3(dmb)]^{2+} \tag{2}$$
$$\text{}^3\text{MLCT(dmb)} \qquad \text{}^3\text{MLCT(MQ)}$$

occurs from the ^{3}MLCT(dmb) excited state, following optical excitation and intersystem crossing (eq 1). Relaxation of the Franck−Condon MLCT(MQ) state is a subpicosecond process.[34] The occurrence of ILET (Scheme 1 and eq 2) was firmly established by previous studies[20,22,23] which have characterized the ILET product $^3[Re^{II}(MQ^{\bullet})(CO)_3(dmb)]^{2+}$ by stationary emission, nanosecond transient visible absorption, and resonance Raman spectroscopy.

ILET Energetics: Cyclic Voltammetry. The driving force ($-\Delta G°$) of the $dmb^{\bullet-} \rightarrow MQ^+$ ILET can be estimated (eq 3) as the difference between the reduction potentials of the MQ^+ and

$$-\Delta G° = E_{MQ} - E_{dmb} - \eta q^2/4\pi\epsilon_o\epsilon_s R \tag{3}$$

dmb ligands (E_{MQ} and E_{dmb}), corrected by the electrostatic term, which accounts for the extra stabilization of $[Re^{II}(MQ^+)(CO)_3(dmb^{\bullet-})]^{2+}$ by the interaction between the separated charges on the two ligands. The potentials E_{MQ} and E_{dmb} are those of the first and second reduction steps of $[Re(MQ^+)(CO)_3(dmb)]^{2+}$ which are localized at the MQ^+ and dmb ligands, respectively.[35] Their values were determined by cyclic voltammetry in those solvents where both reductions are (nearly) chemically and kinetically reversible, Table 1. To estimate the ILET driving force (eq 3), a value of 8.1 Å was used customarily as the upper limit of the charge-separation distance R in $^3[Re^{II}(MQ^+)(CO)_3(dmb^{\bullet-})]^{2+}$. It was calculated from the X-ray structure[36,37] of $[Re^{I}(MQ^+)(CO)_3(bpy)]^{2+}$ as the distance between the center of the inter-ring dmb C−C bond to the center of the pyridinium ring of MQ^+. The values of the static dielectric constant ϵ_s are summarized in Table 1. The symbols q and ϵ_o stand for the electron charge and vacuum permittivity, respectively. The electrostatic term was multiplied by the factor of $\eta = 0.8$ to account for the fact that the excited electron in ^{3}MLCT(dmb) is partly delocalized and the actual charge on $dmb^{\bullet-}$ is less than unity.[38,39] The use of eq 3 involves two main approximations: (i) the difference between the ligand reduction potentials is independent of the Re formal oxidation state and (ii) reduction of the MQ^+ ligand to $MQ^{\bullet}$ does not affect the potential of the subsequent $dmb/dmb^{\bullet-}$ redox couple. This is well substantiated by the similar values of the second reduction potential of $[Re(MQ^+)(CO)_3(dmb)]^{2+}$ and the first reduction potential of $[Re(Etpy)(CO)_3(dmb)]^+$. The values of the first two reduction potentials of $[Re(MQ^+)(CO)_3(dmb)]^{2+}$ and of the estimated ILET driving force in a series of solvents are summarized in Table 1. It follows that the electrostatic term in eq 3 is the main factor responsible for the solvent dependence of $-\Delta G°$.

TABLE 1: ILET Energetics[a]

solvent	MQ^+/MQ (V)	dmb/dmb^- (V)	ΔE (V)	ϵ_s	$-\Delta G°$ (eV)
acetonitrile[b]	−1.10	−1.61	0.51	37.50	0.47
butyronitrile[b]	−1.10	−1.65	0.55	20.30	0.48
benzonitrile[b]	−1.12	−1.69	0.57	25.20	0.51
N,*N*-dimethyl-formamide[b]	−1.20	−1.68	0.48	36.71	0.44
methanol[c]	−1.15	−1.65[e]	∼0.50	32.66	∼0.46
2-ethoxyethanol[b]	−0.86[f]	−1.41[f]	0.55	29.60	0.50
ethylene glycol[c]	−0.93	−1.45	0.52	37.70	0.48
tetrahydrofuran[b]	−1.13	−1.65	0.52	7.58	0.33
$CH_3OCH_2CH_2OCH_3$[b]	−1.15[f]	−1.67[f]	0.52	7.20	0.32
dichloromethane[b]	−1.08	−1.69	0.61	8.93	0.45
1,2-dichloroethane[b]	−1.07	−1.67	0.60	10.36	0.46
pyridine[b]	−1.12	−1.66	0.54	12.40	0.43
dimethyl sulfoxide[b]	−1.14	−1.59	0.45	46.45	0.42
nitromethane[b]	−1.08	−1.65[e]	∼0.57	36.15	∼0.53

[a] $MQ^+/MQ^{\bullet}$ and $dmb/dmb^{\bullet-}$ = the first two reduction potentials of $[Re(MQ^+)(CO)_3(dmb)]^{2+}$, values vs Fc/Fc^+. ΔE = the corresponding potential difference. ϵ_s = static dielectric constant.[40,41] $-\Delta G°$ = ILET driving force estimated using eq 3. [b] 0.1 M Bu_4NPF_6, Pt working electrode. [c] 0.1 M $LiClO_4$, glassy-carbon working electrode. [d] 0.1 M Bu_4NPF_6, dropping Hg working electrode. [e] The potential of the second reduction is experimentally inaccessible. The average value for the $dmb/dmb^{\bullet-}$ potential is reported. [f] Potentials vs Ag pseudoreference electrode.

Kerr-Gate Picosecond Time-Resolved Emission. The ILET driving force can be, in principle, estimated from the time-resolved emission spectra. Such estimates are, however, only very approximate since determination of free-energy changes upon excited-state decay requires fitting of the emission band shape and knowledge of its half-width.[42−44] This is not possible herein because of the low intensity, broadness, and overlap between two emission bands. Hence, only energies of emission band maxima were used.

Shown in Figure 1 is the Kerr-gate time-resolved emission spectrum of $[Re(MQ^+)(CO)_3(dmb)]^{2+}$ in CH_3CN. A broad intense band, which appears immediately after excitation, is centered at ca. 520 nm (measured at 7 ps). It rapidly decays in

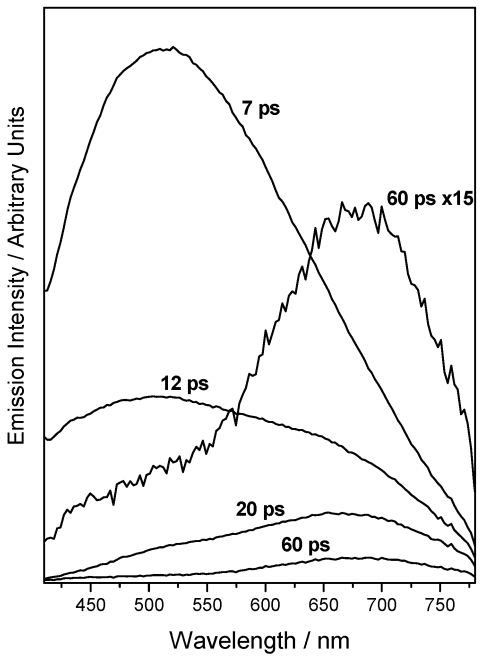

Figure 1. Kerr-gate emission spectrum of $[Re(MQ^+)(CO)_3(dmb)]^{2+}$ measured in a CH_3CN solution. Excited at 400 nm with a laser pulse of a ca. 1 ps duration. The emission is collected at selected time delays after excitation for ca. 4 ps, while the Kerr gate is open. The spectra are not corrected for variations in detector sensitivity at different wavelengths.

intensity, while a much weaker, broad emission band emerges at ~677 nm. In accordance with the previous studies[19,20] of stationary emission of $[Re(MQ^+)(CO)_3(bpy)]^{2+}$, these two emission bands were attributed to the radiative decay of ^{3}MLCT(dmb) and ^{3}MLCT(MQ) excited states, respectively. Similar results were obtained in an ethylene glycol solution where $[Re(MQ^+)(CO)_3(dmb)]^{2+}$ shows an initial emission at 515 nm, which converts into a weak emission at ca. 660 nm. The ILET driving force values estimated as a difference between the ^{3}MLCT(dmb) and ^{3}MLCT(MQ) emission maxima are 0.55 and 0.53 eV in CH_3CN and ethylene glycol, respectively. These values are in good agreement with the electrochemical estimates (Table 1).

The 520 nm emission band of $[Re(MQ^+)(CO)_3(dmb)]^{2+}$ is very similar to the 535 nm (measured at 5 and 10 ps) band seen in the Kerr-gate time-resolved emission spectrum of the reference complex $[Re(Etpy)(CO)_3(dmb)]^+$, in accordance with their common origin in a ^{3}MLCT(dmb) state. The latter band is, however, persistent on the picosecond time scale because of the absence of the ILET deactivation pathway. The 535 nm band also occurs in the stationary emission spectrum[45] of $[Re(Etpy)(CO)_3(dmb)]^+$.

The observation that $[Re(MQ^+)(CO)_3(dmb)]^{2+}$ shows at early times a typical ^{3}MLCT(dmb) emission that decays on the ILET time scale confirms that ILET occurs from the triplet state, after an intersystem crossing (eq 1b) from the optically populated ^{1}MLCT(dmb) state. It can be estimated[43] that the ^{3}MLCT(dmb) precursor state lies ca. 18600 cm^{-1} above the ground state. The 400 nm (25000 cm^{-1}) excitation thus produces the ^{3}MLCT(dmb) state vibrationally excited by about 6400 cm^{-1}. Dissipation of this extra energy has to follow and may influence the ILET process itself, vide infra.

Solvent Dependence of the ILET Rate. The rate of the $dmb^{\bullet-} \rightarrow MQ^+$ ILET was determined in a series of solvents from time-resolved visible absorption spectra using the procedure described previously.[23] The same spectral pattern (Figure 2) was seen in all the solvents measured: a weak, decaying unresolved absorption between ca. 425 and 475 nm due to the $dmb^{\bullet-}$ chromophore and a strong, broad band at around 630 nm that corresponds to the $MQ^{\bullet}$ ligand of the ILET product.[23] The presence of an isosbestic point between 490 and 500 nm and the identical kinetics of the rise and decay of the absorption between 425 and 475 nm and between 600 and 630 nm, respectively, manifest that ILET occurs as a direct conversion between the ^{3}MLCT(dmb) and ^{3}MLCT(MQ) excited states (eq 2). It should be noted that the 630 nm band is in part formed within the instrument time resolution due to a direct population of the ^{3}MLCT(MQ) state, Scheme 1 and eq 1c. In a separate study[34] of $[Re(Cl)(CO)_3(MQ^+)_2]^{2+}$ we found that relaxation of the FC-^{1}MLCT(MQ) state is a subpicosecond process which does not interfere with the ILET kinetics studied herein.

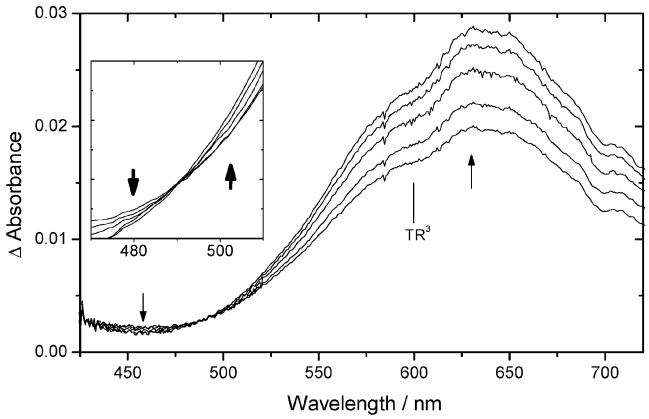

Figure 2. Picosecond time-resolved absorption spectra of $[Re(MQ^+)(CO)_3(dmb)]^{2+}$ in CH_3CN measured at 2, 4, 8, 16, and 30 ps after 400 nm, ca. 250 fs excitation. The spectra evolve in the direction of the arrows. The inset shows details of the isosbestic behavior in the 470−510 nm region. TR^3: the line marks the 600 nm probe wavelength used in the TR^3 experiments.

The ILET time constants were measured from exponential fits of the transient absorption at several probe wavelengths within the 630 nm band. The values obtained in a variety of solvents are summarized in Table 2, together with the estimated driving force values and relevant solvent properties. ILET time constants fall in the 8−18 ps range, showing only a very small solvent dependence.

Kerr-Gate Picosecond TR^3. To investigate structural changes upon ILET, vibrational dynamics of the ILET product $^3[Re^{II}(MQ^{\bullet})(CO)_3(dmb)]^{2+}$, and the dissipation of the ca. 0.5 eV excess energy released during ILET, we have measured picosecond TR^3 spectra of $[Re(MQ^+)(CO)_3(dmb)]^{2+}$, Figure 3. The Kerr gate was used to minimize the interference from the strong emission that would normally preclude any TR^3 measurements. The sample solutions were excited at 400 nm to trigger the ILET process, and the TR^3 spectra were measured using the 600 nm probe wavelength which is in resonance with the absorption band of the $MQ^{\bullet}$ chromophore of the ILET product $^3[Re^{II}(MQ^{\bullet})(CO)_3(dmb)]^{2+}$, Figure 2. Hence, only the Raman bands due to $MQ^{\bullet}$ vibrations appear in the spectra, while no bands were seen in the ν(CO) region (not shown in Figure 3). TR^3 bands were assigned according to previous studies[22,53] of the stationary and transient resonance Raman spectra of $[Re(MQ^+)(CO)_3(bpy)]^{2+}$, its reduced form $[Re(MQ^{\bullet})(CO)_3(bpy)]^+$, Ru^{II} and Os^{II} complexes containing an $MQ^{+/\bullet}$ ligand, and the *N*,*N*′-dimethyl-4,4′-bipyridine radical cation and biphenyl anion. The positions and assignments of Raman bands of both the ground-state $[Re(MQ^+)(CO)_3(dmb)]^{2+}$ and the ILET product $^3[Re(MQ^+)(CO)_3(dmb)]^{2+}$ are summarized in Table 3.

TABLE 2: Solvent Dependence of ILET Dynamics and Relevant Solvent Properties[a]

solvent	τ (ps)	k_{ILET} (10^{10} s^{-1})	$-\Delta G°$ (eV)	$1/\epsilon_{op} - 1/\epsilon_s$	$\langle\tau_s\rangle$ (ps)	IP (eV)	LUMO (eV)	V_{el} (cm^{-1})	λ (W m^{-1} K^{-1})	κ (10^{-8} m^2 s^{-1})
acetonitrile	8.3 ± 0.4	12.0	0.47	0.529	0.26[b]	12.20	5.77	1.1	0.188	10.68
propionitrile	9.4 ± 0.4	10.6		0.501	1.15[c]	11.84			0.169	9.82
butyronitrile	10.4 ± 0.8	9.62	0.48	0.474	1.85[d]	11.20			0.169	9.51
valeronitrile	10.3 ± 0.7	9.71		0.462	3.60[e]				0.166	9.16
isobutyronitrile	8.7 ± 0.5	11.5		0.483	1.88[e]	11.30			0.162	9.33
benzonitrile	9.0 ± 0.7	11.1	0.51	0.390	5.10[b]	9.70	2.44	2.8	0.148	8.40
dichloromethane	10.5 ± 1.0	9.52	0.45	0.383	0.56[b]	11.32	4.19	2.0	0.139	8.74
dichloromethane-d_2	10.6 ± 1.1	9.43								
1,2-dichloroethane	8.8 ± 0.9	11.4	0.46	0.384		11.04			0.135	8.40
formamide	8.5 ± 0.6	11.8		0.469	5.0[b]	10.16			0.353	12.12
N-methylformamide[h]	9.2 ± 0.3	10.9		0.484	5.7[b]	9.83			0.203	9.21
DMF[h]	9.5 ± 0.5	10.5	0.44	0.463	0.92[b]	9.12			0.184	9.48
methanol	11.8 ± 0.6	8.26	~0.47	0.537	5.0[b]	10.85			0.201	10.19
methanol-d_1	11.7 ± 1.0	8.26			7.46[f]					
methanol-d_4	12.0 ± 0.7	8.33			7.77[f]					
ethylene glycol	14.0 ± 1.6	7.14	0.48	0.462	15.0[b]	10.16			0.256	8.66
2-ethoxyethanol	12.4 ± 1.2	8.06	0.52	0.471		9.60			0.175	8.06
THF	16.1 ± 1.2	6.21	0.33	0.375	0.94[b]	9.38	6.21	1.1	0.121	8.21
$CH_3OCH_2CH_2OCH_3$	17.5 ± 1.3	5.71	0.33	0.586		9.30			0.142	7.90
pyridine	9.1 ± 0.7	11.0	0.43	0.360		9.25			0.165	9.95
DMSO[h]	9.7 ± 0.7	10.3	0.42	0.436	1.79[b]	9.10			0.157	7.50
nitromethane	9.6 ± 0.7	10.4	~0.53	0.498	0.41[g]	11.08			0.207	1.07

[a] τ and k_{ILET} = time and rate constants of ILET measured by time-resolved visible absorption spectroscopy. $-\Delta G°$ = ILET driving force from Table 1. ϵ_s = dielectric constant.[40] ϵ_{op} = optical dielectric constant.[40] $\langle\tau_s\rangle$ = average solvent relaxation time. IP = solvent ionization potential.[46] LUMO = solvent LUMO energy.[41] V_{el} = through-solvent electronic coupling determined for electron transfer in organic C-shaped molecules.[41] λ = thermal conductivity.[47] κ = temperature diffusivity ($\kappa = \lambda/dC_p$, where d is density[40] and C_p thermal heat capacity[46]). [b] Reference 48. [c] Averaged values from refs 49 and 50. [d] Averaged values from ref 49. [e] Reference 49. [f] Reference 51. [g] Reference 52. [h] The following values were determined from the biexponential kinetic fit which took into account the fast back-reaction:[26] 9.9 ± 0.4, 10.3 ± 0.4, and 10.5 ± 0.6 ps in *N*-methylformamide, DMF, and DMSO, respectively.

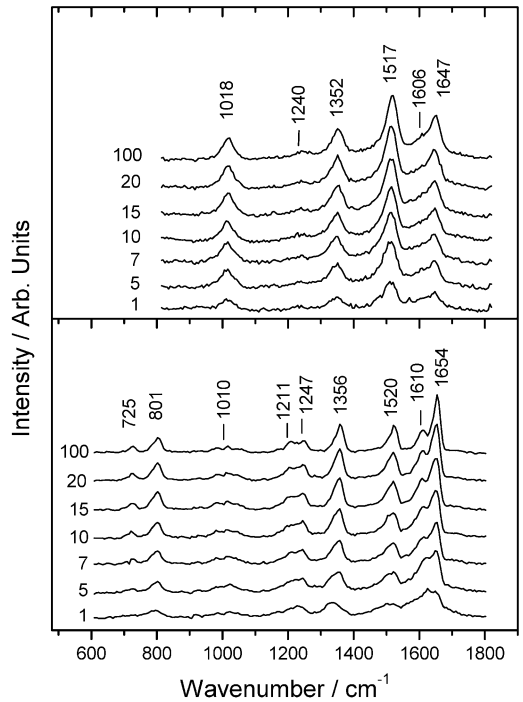

Figure 3. TR^3 spectra of [Re(MQ$^+$)(CO)$_3$(dmb)]$^{2+}$ measured in CH_3CN at selected time delays after 400 nm, ca. 1 ps excitation. Interfering luminescence was eliminated by a ~4 ps Kerr gate. Time delays in picoseconds are shown on the left. Top: probed at 600 nm. Bottom: probed at 400 nm.

The TR^3 spectrum of [Re(MQ$^+$)(CO)$_3$(dmb)]$^{2+}$ obtained in a CH_3CN solution between 1 and 500 ps after ca. 1 ps laser pulse excitation is shown in Figure 3 (top). The TR^3 spectra obtained in other solvents studied (BuCN, MeOH, ethylene glycol, and 1,2-dichloroethane) are very similar. The positions of the Raman bands measured at long time delays (>100 ps) are almost solvent-independent, lying within ±2 cm^{-1} of the values measured in CH_3CN. Some ^{3}[Re^{II}(MQ$^•$)(CO)$_3$(dmb)]$^{2+}$ is formed within the instrument time resolution (≤1 ps) by direct Re → MQ$^+$ MLCT optical excitation at 400 nm, vide supra. This is manifested by the presence of the corresponding peaks already in the spectrum measured at 1 ps. Then, the integrated intensities of the Raman bands increase with time constants (8 ± 3 and 12 ± 3 ps in CH_3CN and ethylene glycol, respectively) which are, within experimental accuracy, identical with the ILET time constants measured by time-resolved visible absorption in these solvents. This observation clearly demonstrates that the TR^3 bands indeed belong to the ILET product ^{3}[Re^{II}(MQ$^•$)(CO)$_3$(dmb)]$^{2+}$. Figure 3 (bottom) displays TR^3 spectra probed at 400 nm. They also show only peaks due to the reduced MQ$^•$ ligand in the ^{3}[Re(MQ$^•$)(CO)$_3$(dmb)]$^{2+}$ ILET product, Table 3. However, the intensity pattern differs from that observed in the spectra probed at 600 nm. In addition to the bands observed in the spectra probed at 600 nm, the 400 nm spectra show weak bands at 725, 801, and 1211 cm^{-1}, which are attributed[22,53] to ν(CC), ν(CC)/ν(CN)/ν(N$^+$CH$_3$), and δ(CCH) vibrations of MQ$^•$, respectively. The differences between the 400 and 600 nm probed spectra are caused by the different origins of the resonance intensity enhancements, that is, in the 630 nm (broad) and 370 nm (sharp)[20] absorption bands, respectively. The TR^3 spectral patterns obtained with λ_{pump} = 350 nm and λ_{probe} = 400 nm and λ_{pump} = 400 nm and λ_{probe} = 350 nm are very similar to those pumped and probed at 400 nm, although the signal intensities are generally much weaker and the signal/noise ratio is higher.

Neither of the early TR^3 spectra probed in the near-UV region (400 or 350 nm) show any peaks due to the dmb$^{•-}$ ligand of the ^{3}[Re(MQ$^+$)(CO)$_3$(dmb$^{•-}$)]$^{2+}$ precursor. This can be understood in view of the fact that the TR^3 spectra of the reference complex [Re(Etpy)(CO)$_3$(dmb)]$^+$ show only very weak Raman bands which, moreover, slowly grow in during the first ~15

TABLE 3: Steady-State Resonance Raman (rR) and Picosecond TR³ Spectra of $[Re(MQ^+)(CO)_3(dmb)]^{2+}$ [a]

	TR³, pump/probe					
rR	400/600	400/400	400/350[g]	350/400	$\Delta\nu$	assignment
2033m (0.43)						A′(1) ν(CO)
1649s (1)	1647s (1)	1654vs (1)	1649s	1654s		MQ $\nu(CC)_{ir}/\nu(CC)$[b,d,e]
1618vs (1.98)			1618sh			dmb $\nu(CC_{Me})/\nu(CC)_{ir}/\nu(CN)$[c]
	1606sh	1610m (0.38)		1608m		MQ $\nu(CC)_{ir}$[f]
1555w (0.18)						dmb $\nu(CC)/\nu(CN)/\delta(CCH)$[c]
1528w (0.18)	1516vs (1.48)	1520m (0.46)	1524m	1521m	−10	MQ $\nu(CN)/\delta(CCH)/\nu(CC)$[b,d,e]
1492m (0.37)						dmb $\delta(CCH)/\nu(CC)/\nu(CC)_{ir}/\nu(CN)$[c]
1321m (0.37)						dmb $\delta(CCH)/\nu(CC)_{ir}$[c]
1299s (0.71)	1352s (0.76)	1356m (0.49)	1365m	1357m	+55	MQ $\nu(CC)_{ir}/\delta(CCH)/\nu(CC)$[b,d,e]
1231w (0.29)	1240w[h] (0.21)	1247w (0.22)	1244w	1246w	+16	MQ $\nu(N^+Me)/\nu(CC)/\delta(CCH)$[b,d]
1193w (0.36)		1211w (0.19)	1212w	1209w	+18	MQ $\delta(CCH)/\nu(CC)$[b,d,e] or dmb $\delta(CCH)$[c]
1071w (0.34)				*j*		MQ $\nu(CN)/\nu(CC)/\delta(CCH)$[d,e]
1033s (1.04)			1034w	*j*		dmb $\nu(CC)/\delta(CCH)$[c]
1019s (0.91)				*j*		MQ $\nu(CC)/\delta(CCC)$[b,e]
	1018m (0.50)	1010vw (0.11)		*j*		MQ $\delta(CCN)/\nu(CN)$[b]
	j	801w (0.27)	811w	*j*		MQ $\nu(CC)/\nu(CN)/\nu(N^+Me)$[b,d]
732vw (0.13)	*j*	725vw (0.11)		*j*	−7	MQ $\nu(CC)/\delta(CCC)$[b,e]
494s (0.85)	*j*		*j*	*j*		tentatively $\nu(ReN)/\nu(ReC)/\delta(NReN)$[i]
378m (0.56)	*j*		*j*	*j*		tentatively $\nu(ReN)/\nu(ReC)/\delta(NReN)$

[a] Raman band positions are in wavenumbers (cm^{-1}). Intensities relative to the band at 1649 cm^{-1} in parentheses. $\Delta\nu$ is the difference between excited- and ground-state Raman peaks. MQ denotes vibrations of the MQ^+ and $MQ^\bullet$ ligands in the rR and TR³ spectra, respectively. rR spectra were measured using 514.5 nm excitation. TR³ wavenumbers taken as average values of 400/600 and 400/400 nm measurements. [b] Reference 22. [c] References 55−57. [d] Reference 58. [e] Reference 59. [f] Reference 60. [g] Approximate value due to noisy spectra. [h] Very broad, could encompass two bands. [i] Reference 61. [j] Not investigated. [k] Band may arise from preresonance with the near-UV intra-$dmb^{\bullet-}$ electronic transitions.

TABLE 4: TR³ Band Shift and Narrowing Dynamics (ps)[a]

	position (cm^{-1})				width (fwhm) (cm^{-1})			
Raman band	1516	1352	1018	801	1516	1352	1018	801
acetonitrile	23 ± 3 (13 ± 2)	16 ± 4 (11 ± 2)	15 ± 6	(5 ± 1)	17 ± 5 (5 ± 0.6)	11 ± 4 (8 ± 4)	13 ± 4 (15 ± 5)	(5 ± 0.6)
butyronitrile	18 ± 2	19 ± 2	14 ± 2				18 ± 3	
methanol	15 ± 2	18 ± 4			9 ± 2			
ethylene glycol	15 ± 3 (12 ± 1)	12 ± 3 (7 ± 0.4)	11 ± 5	(14 ± 3)	(4 ± 0.4)	5 ± 1 (8 ± 0.6)		(12 ± 3)
1,2-dichloroethane	24 ± 5	36 ± 6	22 ± 8		10 ± 4			

[a] $\lambda_{pump} = 400$ nm, $\lambda_{probe} = 600$ nm (values in parentheses: $\lambda_{pump} = 400$ nm, $\lambda_{probe} = 400$ nm, measured for CH_3CN and ethylene glycol).

ps, manifesting vibrational cooling.[54] This observation indicates that the ^{3}MLCT(dmb) ILET precursor state of $^3[Re^I(MQ^+)(CO)_3(dmb)]^{2+}$ is initially formed vibrationally hot in low-frequency vibrations which are anharmonically coupled to high-frequency ones. This vibrational excitation persists on a time scale that is comparable with that of ILET.

Listed in Table 3 are also differences between the Raman peak wavenumbers of the ground-state $[Re(MQ^+)(CO)_3(dmb)]^{2+}$ and the ILET product $^3[Re(MQ^\bullet)(CO)_3(dmb)]^{2+}$, the latter measured at time delays of 100 ps and longer. The largest shift of +55 cm^{-1} is seen for the 1299 cm^{-1} peak that corresponds to vibration with a large contribution from the MQ inter-ring C−C stretch. This is clearly indicative of the reduction of MQ^+ to $MQ^\bullet$ which has a quinoidal structure where the inter-ring bond is strengthened by π-interaction between the two rings, Scheme 1. The bands at 1193, 1231, and 1528 cm^{-1} also undergo significant shifts. The band at ca. 1609 cm^{-1} seems to be present only in the TR³ spectrum, having no ground-state counterpart. This band possibly corresponds to a vibration with a significant contribution from the inter-ring C−C stretch. It should be noted that the shift of the Raman bands from their ground-state values is virtually instantaneous, occurring within the instrument temporal resolution, that is, <1 ps. It is only the Raman band intensities, not the positions that follow the ILET kinetics.

Close inspection of the TR³ spectra reveals that the Raman peaks undergo small dynamic shifts by 7−9 cm^{-1} to higher wavenumbers and narrowing by 16−25%, which follow single-exponential dynamics. The corresponding time constants are summarized in Table 4. For a given Raman band, the peak positions and widths are inversely proportional, although the experimental points show some scatter. The dynamic peak shift and narrowing demonstrate that the ILET product is initially formed vibrationally excited in low-frequency vibrational modes that are anharmonically coupled[62,63] to high-frequency $MQ^\bullet$ vibrations, slightly decreasing their wavenumbers. As the vibrational cooling proceeds and excited low-lying modes are depopulated, the anharmonic coupling gradually disappears and the Raman peaks shift higher and narrow.[62−64] The corresponding time constant should correspond to intermolecular vibrational energy dissipation into the bulk solvent, away from the first solvation sphere.[65−68] However, in the present case, the intermolecular relaxation dynamics are partly convoluted with those of ILET, since their respective time scales are only a little different. Nevertheless, the time constants of the Raman peak shifts approximately correlate with the heat conductivity and temperature diffusivity of the solvent, as was found before for organic molecules.[65,67,68] Notably, the vibrational relaxation is the slowest in 1,2-dichloroethane, which has not only rather low heat capacity and temperature diffusivity, but also low polarity. Hence, the solvation is weak, not providing an efficient relaxation pathway. Finally, it should be noted that the picosecond TR³ spectrum of $[Re(Cl)(CO)_3(MQ^+)_2]^{2+}$ does not show comparable dynamic effects.[34] In this case, the ^{3}MLCT-(MQ) state is populated only by optical excitation. By comparison, we may conclude that, for $[Re(MQ^+)(CO)_3(dmb)]^{2+}$, it is the ILET process which is responsible for the observed vibrational excitation of the $MQ^\bullet$ ligand.

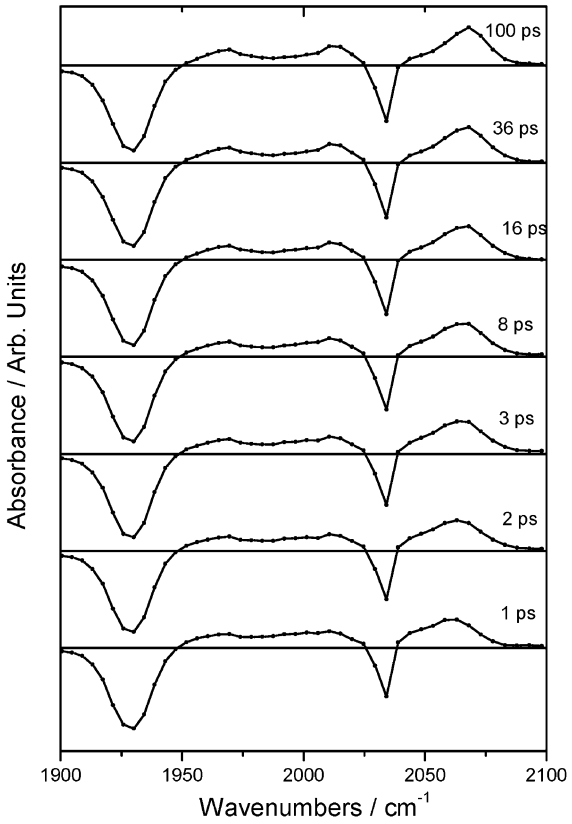

Figure 4. Time-resolved difference infrared spectra of [Re(Etpy)(CO)$_3$(dmb)]$^+$ measured in CH_3CN at selected time delays after 400 nm, ca. 250 fs excitation. Positive bands correspond to the photogenerated species, while the negative bands (bleach) arise from the depletion of the ground-state population. Experimental points are separated by ca. 4 cm^{-1}.

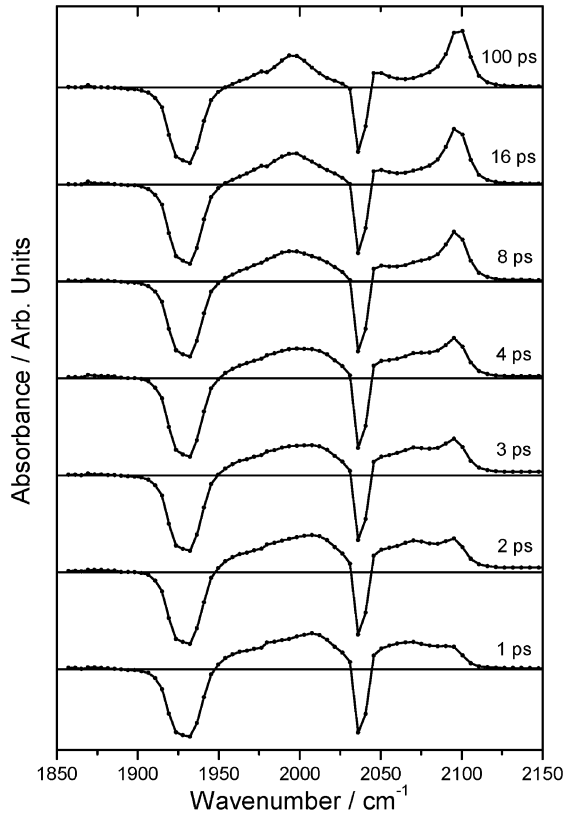

Figure 5. Time-resolved difference infrared spectra of [Re(MQ$^+$)(CO)$_3$(dmb)]$^{2+}$ measured in CH_3CN at selected time delays after 400 nm, ca. 250 fs excitation. (The small discontinuity at 1978 cm^{-1} arises from joining two spectral windows.) Positive bands correspond to the photogenerated species, while the negative bands (bleach) arise from the depletion of the ground-state population. Experimental points are separated by ca. 4 cm^{-1}.

In conclusion, the shifts of the peak wavenumbers of the Raman bands due to MQ$^+$ intraligand vibrations upon ILET demonstrate that MQ$^+$ undergoes large structural rearrangement. The upward shift of the inter-ring ν(CC) vibration and the emergence of the new Raman band at 1609 cm^{-1} due to ν(C═C) vibrations support the quinoidal structure proposed for the MQ$^\bullet$ ligand in the ILET product. Unfortunately, in this study, we were unable to interrogate the inter-ring torsional vibration because of its low wavenumber, expected[69] at ca. 240 cm^{-1}. TR^3 spectroscopy of [Re(MQ$^+$)(CO)$_3$(dmb)]$^{2+}$ and the [Re(Etpy)(CO)$_3$(dmb)]$^+$ reference revealed three dynamic processes associated with ILET: picosecond cooling of the ^{3}MLCT(dmb) precursor, ILET itself, and only a little slower vibrational relaxation (cooling) of the ^{3}MLCT(MQ) ILET product.

Picosecond Time-Resolved IR Spectroscopy. Structural changes and dynamics of the Re(CO)$_3$ moiety following Re → dmb MLCT excitation and ILET were investigated using picosecond TRIR in the spectral region of ν(CO) vibrations. This technique can provide unique structural and dynamical information owing to the high sensitivity of ν(CO) vibrations to the electron density distribution within the complex molecules.[43,45,61,70−72] The picosecond TRIR spectra of the model complex [Re(Etpy)(CO)$_3$(dmb)]$^+$ and of [Re(MQ$^+$)(CO)$_3$(dmb)]$^{2+}$ are shown in Figures 4 and 5, respectively. The IR bands which emerge after excitation of either complex are shifted to higher wavenumbers relative to the corresponding ground-state bands. This overall upward shift of the ν(CO) bands is caused by a decrease of Re → CO π back-donation and increase of OC → Re σ donation upon MLCT excitation.[45] It indicates that all the investigated species are ^{3}MLCT excited states in which the Re(d_π) orbitals are depopulated relative to the ground state and the Re atom can be formally assigned oxidation state II. The band shape of all IR bands investigated herein is Lorentzian, as expected.[73]

The TRIR spectrum of the reference complex [Re(Etpy)(CO)$_3$(dmb)]$^+$ (Figure 4) is attributed to the long-lived ^{3}MLCT(dmb) state ^{3}[Re(Etpy)(CO)$_3$(dmb$^{\bullet-}$)]$^+$. The spectra measured at long time delays (≥100 ps) correspond well to the excited-state IR spectrum measured previously[45] by step scan, using nanosecond excitation, while the bands measured at early times, 10−15 ps, are slightly lower due to anharmonic coupling with highly excited low-frequency vibrations. The highest ν(CO) A′(1) band shifts upon excitation by ca. +32 cm^{-1}, to 2068 cm^{-1}. The low-frequency in-plane A″ and A′(2) ν(CO) vibrations, which are nearly degenerate in the ground state, split upon excitation, giving rise to two distinct bands at ca. 1970 and 2013 cm^{-1}, which are tentatively assigned to A″ and A′(2) vibrations, respectively.[45] The near degeneracy of the A′(2) and A″ vibrations in the ground state results from similar bonding properties of dmb and Etpy to Re, which keep the local symmetry of the Re(CO)$_3$ group close to C_{3v}. The large split between these modes in the ^{3}MLCT(dmb) state ^{3}[Re^{II}(Etpy)(CO)$_3$(dmb$^{\bullet-}$)]$^+$ manifests the pronounced difference between the bonding of the Etpy and dmb$^{\bullet-}$ ligands toward Re, which causes lowering of the local symmetry of the Re(CO)$_3$ unit in the ^{3}MLCT(dmb) excited state to C_s.

The TRIR ν(CO) bands of the ^{3}MLCT(dmb) excited state of [Re(Etpy)(CO)$_3$(dmb)]$^+$ undergo a dynamical narrowing and a shift to higher wavenumbers.[54] The maximum of the A′(1) band at 2068 cm^{-1} shifts by +11.4 ± 0.8 cm^{-1} with a biexponential

dynamics 1.3 ± 0.2 ps (74%) and 11.6 ± 2.1 ps, while its bandwidth decreases by ca. 24% with a time constant of 9.8 ± 1.8 ps. The middle A′(2) band at 2013 cm^{-1} shows a biexponential shift by +15.5 ± 3 cm^{-1}, $\tau = 1 \pm 0.4$ ps (68%), 7.2 ± 1.8 ps (32%) and narrowing. The A″ band at 1970 cm^{-1} also undergoes an upward shift and narrowing, whose quantitative analysis is, however, hampered by overlap with the bleach. This dynamic behavior is analogous to that observed for [Re(Cl)-$(CO)_3$(4,4′-R_2-bpy)] (R = COOH, COOEt) in DMF.[74] This observation demonstrates that the ^{3}MLCT(dmb) state is initially formed vibrationally hot in low-frequency vibrations, which relax on the picosecond time scale. It should be noted that no high-frequency $\upsilon = 1 \rightarrow 2$ ν(CO) hot bands were seen in the TRIR spectra. It follows that the initial energy excess deposited in the ^{3}MLCT(dmb) state upon its population from the ^{1}MLCT(dmb) state is redistributed into the low-frequency modes in less than 1 ps.

Accordingly, all the early dynamics of $^3[Re^{II}(Etpy)(CO)_3(dmb^{\bullet-})]^+$ are attributed to the vibrational relaxation (cooling) of the ^{3}MLCT(dmb) excited state, whose rate is comparable with that of ILET in $^3[Re(MQ^+)(CO)_3(dmb^{\bullet-})]^{2+}$.

The TRIR spectra of $[Re(MQ^+)(CO)_3(dmb)]^{2+}$ consist of two overlapping spectral patterns, one of which decays with time while the other grows in; see Figure 5. The decaying pattern consists of two weak bands at approximately 1970 and 2013 cm^{-1} and a stronger band at ∼2070 cm^{-1} which are identical to the bands observed in the TRIR spectrum of $[Re(Etpy)(CO)_3(dmb)]^+$. Hence, they are attributed to the ^{3}MLCT(dmb) excited state, that is, to the ILET precursor $^3[Re^{II}(MQ^+)(CO)_3(dmb^{\bullet-})]^{2+}$. While these bands decrease, new bands at 1993 (broad) and 2096 cm^{-1} increase in prominence. Close inspection of Figure 5 reveals another growing band that overlaps with the negative bleach at 2034 cm^{-1}. It is manifested by rising absorbance at the high-wavenumber side of the bleach and by a small decrease of the 2034 bleach cm^{-1} relative to the 1930 cm^{-1} bleach. The band maximum can be estimated as ∼2040 cm^{-1}. It appears that this band is weaker than the 1993 cm^{-1} band. The 2096, ∼2040, and 1993 cm^{-1} bands are attributed to the A′(1), A′(2), and A″ ν(CO) vibrations of the ILET product $^3[Re^{II}(MQ^{\bullet})(CO)_3(dmb)]^{2+}$, respectively. This assignment is confirmed by measuring the rise time of the 2096 cm^{-1} band area, 9 ± 1 ps, which is identical with the ILET time constant. The dynamics in the region of the lower two ν(CO) bands, 1960−2050 cm^{-1}, is difficult to analyze quantitatively because of a strong overlap between the bands and their dynamic shifts. Nevertheless, it is obvious that all the ν(CO) bands shift to higher wavenumbers upon ILET. A″ and A′(2) retain their separation. The relative intensity of A′(2) decreases while A′(1) increases. The large magnitude of the shift of the ν(CO) bands (ca. +26 cm^{-1} on average) indicates a higher charge separation in the $^3[Re^{II}(MQ^{\bullet})(CO)_3(dmb)]^{2+}$ product as compared with the $^3[Re^{II}(MQ^+)(CO)_3(dmb^{\bullet-})]^{2+}$ precursor state. This is caused by a predominant localization of the excited electron on the remote pyridinium ring of the $MQ^{\bullet}$ ligand, in contrast to the partial π delocalization in the Re($dmb^{\bullet-}$) chelate ring of $^3[Re^{II}(MQ^+)(CO)_3(dmb^{\bullet-})]^{2+}$. The change in the IR ν(CO) spectral pattern upon ILET thus manifests a pronounced structural change of the $Re(CO)_3$ unit. The upward band shifts reflect shortening of C≡O bonds, while the change in relative intensities suggests changes of OC−Re−CO bond angles that result in changing compositions of ν(CO) normal coordinates.[45,72]

The TRIR spectra also reveal the presence of two kinds of vibrational excitation related to ILET. First, the decay of the ∼2070 cm^{-1} band of the ^{3}MLCT(dmb) precursor state is accompanied by a blue shift similar to that observed for the $[Re(Etpy)(CO)_3(dmb)]^+$ model. Second, the $^3[Re(MQ^{\bullet})(CO)_3(dmb)]^{2+}$ ILET product undergoes vibrational cooling on a time scale comparable with that of ILET itself: The 2096 cm^{-1} band shifts to higher wavenumbers by about 4 cm^{-1} with an apparent time constant of ca. 8 ± 1 ps. Moreover, an initial 8 ± 1 ps upward shift is indicated for the A″ band at 1993 cm^{-1}. These dynamics are again attributed to anharmonic coupling between the ν(CO) modes of the ILET product with low-frequency modes which accept the ca. 0.5 eV excess energy released during ILET.

The conversion of the ^{3}MLCT(dmb) ν(CO) spectral pattern into that of the ^{3}MLCT(MQ) state seen in TRIR spectra provides very conclusive evidence for ILET. Similarly to TR^3 experiments, TRIR shows three kinds of dynamics convoluted with ILET: (i) cooling of the precursor state, (ii) ILET accompanied by an "instantaneous" change in the frequencies of high-frequency vibrations, and (iii) cooling of the ILET product.

Discussion

Time-resolved spectroscopic experiments and energetic considerations offer the following mechanistic picture of ILET: Optical excitation prepares a ^{3}MLCT(dmb) excited state, $^3[Re(MQ^+)(CO)(dmb^{\bullet-})]$, that is highly excited in low-frequency intramolecular, solute−solvent and first-solvation-shell vibrational modes. The $dmb^{\bullet-} \rightarrow MQ^+$ ILET occurs from this hot ^{3}MLCT(dmb) state on a picosecond time scale alongside its vibrational cooling. The ILET driving force is solvent-dependent, 0.3−0.5 eV. ILET is accompanied by large intramolecular structural changes of both the MQ and $Re(CO)_3$(dmb) moieties and by a decrease of electron density on the $Re(CO)_3$ fragment. The ILET product, that is, the ^{3}MLCT(MQ) state $^3[Re^{II}(MQ^{\bullet})(CO)_3(dmb)]^{2+}$, is formed vibrationally excited in low-frequency modes, which accept the released energy. Vibrational cooling of the $^3[Re^{II}(MQ^{\bullet})(CO)_3(dmb)]^{2+}$ product occurs on a time scale only slightly longer than that of the ILET itself.

ILET dynamics are surprisingly little dependent on the solvent. The time constant ranges from 8.3 to 17.5 ps in CH_3CN and $CH_3OCH_2CH_2OCH_3$, respectively. The small variations in the ILET rate cannot be attributed to any particular solvent property such as the solvent function $1/\epsilon_{op} - 1/\epsilon_s$, which determines the outer-sphere reorganization energy, or the average solvation time $\langle\tau_s\rangle$. (The small slowing down of ILET on going from MeOH to ethylene glycol could be caused by slower solvation in the latter.)

We have also explored the possibility that ILET occurs through the solvent molecules which intervene between the $dmb^{\bullet-}$ and MQ^+ ligands.[27,41] In this case, we would expect a correlation either with the solvent ionization potential or with the LUMO energy, for the through-solvent hole- or electron-transfer superexchange mechanism, respectively.[41] Again, no correlation was found, Table 2. The through-solvent electron transfer has recently been found for organic C-shaped electron-transfer dyads, where the electron-transfer rate correlates with the LUMO energy.[41] Analysis of these data provided values of the through-solvent electronic coupling for several of the solvents used herein, Table 2. However, they are much smaller than the values estimated for ILET (vide infra) and do not correlate with the ILET time constants. The through-solvent mechanism is thus excluded. Instead, we propose that ILET follows a through-bond superexchange mechanism, whereby the electronic coupling is provided by the Re atom.

The only way in which the solvent appears to influence the ILET dynamics is by changing the driving force. ILET occurs

in the Marcus normal region, and its rate constant increases with increasing driving force. The data in Tables 1 and 2 show that solvent variations of the driving force easily explain the low ILET rates observed in ethers, where the driving force is much lower than in other solvents. However, driving force changes do not account for other subtle variations observed, namely, for the rates measured in alcohols, where ILET is slower than in aprotic solvents, except ethers. Specific solute−solvent interactions, namely, hydrogen bonding with the CO ligands, can operate in alcohols. In this respect, $CH_3OCH_2CH_2OH$ provides an interesting example, having both OH and ether functional groups. The driving force and the time constant are typical for alcohols, demonstrating a predominant solvation through the OH end.

In fact, ILET in ^{3}[Re(MQ$^+$)(CO)$_3$(dmb$^{\bullet-}$)]$^{2+}$ is surprisingly fast, its rate in many solvents being only a little slower than that of the solvent relaxation. In ethylene glycol, ILET is even faster than solvent relaxation. To interpret the ILET dynamics, a reliable estimate of the total reorganization energy λ is needed. Previously, we have used λ values in the 0.6−0.8 eV range.[23] This estimate was based on the published data for the bpy$^{\bullet-}$ → MV^{2+} electron transfer in [Ru(bpy)$_2$(bpy-MV^{2+})]$^{4+}$, taking into account only the dmb and MQ$^+$ units. The present TRIR study shows that the actual reorganization energy has to be larger because of the contribution from the large structural changes of the Re(CO)$_3$ unit. Moreover, reduction of MQ$^+$ seems to cause larger structural changes than that of MV^{2+}.[36] Therefore, λ values are expected to lie in the range 1.0−1.2 eV or even higher. The corresponding values of the free energy of activation $\Delta G^{\ddagger}$, eq 4, range from 0.070 to 0.111 eV (that is, 565−895 cm^{-1}), using $\Delta G^\circ = -0.47$ eV (in CH_3CN) and $T = 293$ K.

$$\Delta G^{\ddagger} = (\lambda + \Delta G^\circ)^2/4\lambda \qquad (4)$$

To estimate the electronic coupling V_{el}, we have used the data for fast-relaxing CH_3CN (260 fs), where a mostly nonadiabatic behavior can be assumed even if V_{el} is large. This situation is described by eq 5,[7,75,76] where k_{NA} is the electron-

$$k_{ILET} = \frac{k_{NA}}{1 + H_A} \qquad (5)$$

transfer rate constant of a completely nonadiabatic process (eq 6) and H_A is the adiabaticity parameter (eq 7). Using $k_{ILET} = 1.20 \times 10^{11}$ s^{-1}, $\langle\tau_s\rangle = 260$ fs in CH_3CN, and a lower estimate of $\lambda = 1.0$ eV, we obtain $V_{el} = 1.62 \times 10^{-2}$ eV (131 cm^{-1}).

$$k_{NA} = \frac{2\pi V_{el}^{\ 2}}{\hbar(4\pi\lambda k_B T)^{1/2}} \exp[-(\lambda + \Delta G^\circ)^2/4\lambda k_B T] \qquad (6)$$

$$H_A = \frac{4\pi V_{el}^{\ 2}\langle\tau_s\rangle}{\hbar\lambda} \qquad (7)$$

The adiabaticity parameter H_A is then calculated as 1.3. It follows that ILET is partly adiabatic even in the fast-relaxing CH_3CN, becoming fully adiabatic in "slower" solvents; $\langle\tau_s\rangle \geq 5$ ps, where $H_A \geq 25$. For $H_A \gg 1$, eqs 5−7 can be combined to give eq 8, which predicts adiabatic ILET time constants

$$k_{ILET} = \frac{1}{\langle\tau_s\rangle}\left[\frac{\lambda}{16\pi k_B T}\right]^{1/2} \exp[-(\lambda + \Delta G^\circ)^2/4\lambda k_B T] \qquad (8)$$

($\tau_{ILET} = 1/k_{ILET}$) of $18.2\langle\tau_s\rangle$ for $\lambda = 1.0$. Inspection of Table 2 clearly shows that ILET is actually much faster than predicted. For example, a τ_{ILET} value of ∼91 ps is expected for solvents with a 5 ps relaxation time while values in the range 8.5−11.8 ps were measured for C_6H_5CN, formamide, *N*-methylformamide, and MeOH. The 14 ps ILET time constant in ethylene glycol is ∼20 times shorter than that predicted from eq 8. It should be noted that, using $\lambda > 1$, which is quite possible, would give $V_{el} \gg 130$ cm^{-1} and an adiabatic behavior even in CH_3CN. The discrepancy between the experimental and predicted time constants would then be even higher. Obviously, ILET is much faster than predicted by conventional Marcus theory, which assumes that the reacting system reaches the transition state along a solvation coordinate, while the state from which the electron transfer occurs maintains a thermal equilibrium. Clearly, this is not the case of the ILET reaction studied herein. It has been amply demonstrated above by TR^3 and TRIR spectra that 400 nm excitation initially produces the ^{3}MLCT(dmb) precursor state in an unequilibrated manifold of highly excited low-frequency vibrational levels that are anharmonically coupled to high-frequency vibrations. Specific solvent vibrational modes of the first solvation sphere are excited as well. The extra energy deposited into the reactive ^{3}MLCT(dmb) state, ca. 6400 cm^{-1}, is much higher than the estimated range of activation free energy, 565−895 cm^{-1}, well capable to promote intramolecular vibrational excitation that would overcome the barrier. In fact, activation of intramolecular vibrations is necessary to accomplish the large structural reorganization of the MQ$^{\bullet}$ ligand and the Re(CO)$_3$ unit that accompanies ILET. Considering that ILET occurs in the Marcus normal region, this situation can be, in principle, treated by the Sumi−Marcus model.[77] It describes electron transfer as a two-dimensional process that occurs along solvent *and* intramolecular coordinates, the latter corresponding to low-frequency vibrations treated classically. Provided that the vibrational motion along the intramolecular coordinate occurs much faster than solvation, the electron-transfer dynamics become largely independent of the solvent dynamics. The inclusion of intramolecular vibrations effectively increases the driving force. As a consequence, the free energy of activation will decrease, accelerating the reaction beyond the predictions of classical Marcus theory of adiabatic electron transfer.[6,7,77−80] These qualitative conclusions agree well with the experimental observations discussed above. The predominant role of intramolecular vibrations also explains the observation[20] that ILET occurs even in a glass at 77 K, provided the driving force is sufficient.

In conclusion, the ulrafast ILET rate found for [Re(MQ$^+$)(CO)$_3$(dmb)]$^{2+}$ originates in the combination of the large electronic coupling provided by the Re atom and activation of intramolecular vibrations in the precursor state. Large coupling makes ILET adiabatic, while it is promoted by fast intramolecular motions in the precursor state, instead of much slower solvent fluctuations. Similar involvement of intramolecular vibrations[77,78] was suggested, for example, in the case of back electron transfer in mixed-valence complexes,[81] photoreduction of rhodamine 6G in amine solutions,[82] or intramolecular electron transfer in porphyrin−metal(terpyridine) dyads, whose rate was also found[83] comparable to the solvent relaxation time. The rhodamine 6G photoreduction even seems to occur essentially independently of solvation, with an ultrafast rate of 80−160 fs.[82]

Finally, it is interesting to note that ILET in Os → bpy ^{3}MLCT excited states ^{3}[Os(bpy)$_2$(bpy$^{\bullet-}$)]$^{2+}$ and ^{3}[Os(bpy)(bpy$^{\bullet-}$)(4-amido-bpy)]$^{2+}$ occurs on a time scale similar to that established herein for [Re(MQ$^+$)(CO)$_3$(dmb)]$^{2+}$. Time constants of 8.7 and 1.5 ps were determined[11] for the bpy$^{\bullet-}$ → bpy and

$bpy^{\bullet-} \rightarrow$ 4-amido-bpy ILET in the above two Os complexes, respectively. Interligand electronic coupling V_{el} values were roughly estimated to lie in the range 2.5×10^{-2} to 1.1×10^{-1} eV, similar to the value considered herein. These relatively large coupling values suggest[11] that ILET in these Os complexes is adiabatic even in CH_3CN. A similar value of electronic coupling, $\sim 2.5 \times 10^{-2}$ eV, was estimated for ILET (electron hopping) between 4,4′-$(COOH)_2$-2,2′-bpy and 4,4′-$(COOH)_2$-2,2′-$bpy^{\bullet-}$ ligands in the MLCT excited states of Ru(4,4′-$(COOH)_2$-2,2′-$bpy)_2(NCS)_2$], resulting in the adiabaticity parameter of 95 in MeOH. This large value again points to an adiabatic ILET mechanism.[12] Interestingly, much smaller coupling values, 5.5×10^{-3} to 7.6×10^{-3} eV, were determined spectroscopically for py-PTZ $\rightarrow$ bpy ILET in $[Re^{I}(py\text{-}PTZ)(CO)_3(bpy)]^+$ and related polypyridine complexes (py-PTZ = 10-(4-picolyl)phenothiazine).[84] These much smaller values, as compared with that of $^3[Re^{II}(MQ^+)(CO)_3(dmb^{\bullet-})]^{2+}$, can reflect the difference in the oxidation state of the Re atom, which mediates the coupling, I and II, respectively. It follows that strong electronic coupling and adiabaticity can accelerate ILET between ligands that are directly connected by a metal atom. The actual magnitude of the electronic coupling will depend on the particular metal atom, its oxidation state, and, presumably, also the ancillary ligands.

Conclusions

Optical excitation of $[Re(MQ^+)(CO)_3(dmb)]^{2+}$ triggers an ultrafast $dmb^{\bullet-} \rightarrow MQ^+$ ILET which occurs from vibrationally hot Re $\rightarrow$ dmb ^{3}MLCT excited-state $^3[Re^{II}(MQ^+)(CO)_3(dmb^{\bullet-})]^{2+}$. It is a (partly) adiabatic process which becomes fully adiabatic in solvents with relaxation times longer than ca. 5 ps. The ILET dynamics is predominantly controlled by low-frequency intramolecular vibrations that are anharmonically coupled to high-frequency modes, instead of solvent fluctuations. ILET is accompanied by major structural reorganization of the $MQ^{\bullet}$ ligand and the $Re(CO)_3$ unit. The predominant contribution of intramolecular vibrations to the reaction coordinate, in combination with large electronic coupling, accelerates ILET to such an extent that it becomes only slightly slower than solvation. This, together with the dominance of inner reorganization energy over the outer reorganization, makes the ILET rate only weakly solvent-dependent. Variations in the driving force appear to be the only major way in which solvents influence the ILET dynamics. The ILET product $^3[Re^{II}(MQ^{\bullet})(CO)_3(dmb)]^{2+}$ is initially formed vibrationally hot. Intermolecular vibrational energy transfer to the solvent bath follows on a picosecond time scale. Large electronic coupling combined with vibrational activation of the reactant appears to be a way to accelerate intramolecular electron-transfer reactions in the Marcus normal region.

Acknowledgment. Funding by the Engineering and Physical Sciences Research Council is gratefully appreciated.

References and Notes

(1) Ratner, M. A.; Jortner, J. In *Molecular Electronics*; Jortner, J., Ratner, M., Eds.; Blackwell Science Ltd.: Oxford, 1997; p 5.
(2) Barbara, P. F.; Meyer, T. J.; Ratner, M. A. *J. Phys. Chem.* **1996**, *100*, 13148.
(3) Winkler, J. R.; Di Bilio, A. J.; Farrow, N. A.; Richards, J. H.; Gray, H. B. *Pure Appl. Chem.* **1999**, *71*, 1753.
(4) Qu, P.; Meyer, G. J. In *Electron Transfer in Chemistry*; Balzani, V., Ed.; Wiley-VCH: Weinheim, Germany, 2001; Vol. IV, p 353.
(5) Marcus, R. A. *Angew. Chem., Int. Ed. Engl.* **1993**, *32*, 1111.
(6) Marcus, R. A.; Sutin, N. *Biochim. Biophys. Acta* **1985**, *811*, 265.
(7) Bixon, M.; Jortner, J. In *Electron Transfer—From Isolated Molecules to Biomolecules. Part I. Advances in Chemical Physics*; Jortner, J., Bixon, M., Eds.; J. Wiley and Sons, Inc.: New York, 1999; Vol. 106, p 35.
(8) Sikes, H. D.; Smalley, J. F.; Dudek, S. P.; Cook, A. R.; Newton, M. D.; Chidsey, C. E. D.; Feldberg, S. W. *Science* **2001**, *291*, 1519.
(9) Pogge, J. L.; Kelley, D. F. *Chem. Phys. Lett.* **1995**, *238*, 16.
(10) Cushing, J. P.; Butoi, C.; Kelley, D. F. *J. Phys. Chem. A* **1997**, *101*, 7222.
(11) Shaw, G. B.; Brown, C. L.; Papanikolas, J. M. *J. Phys. Chem. A* **2002**, *106*, 1483.
(12) Waterland, M. R.; Kelley, D. F. *J. Phys. Chem. A* **2001**, *105*, 4019.
(13) Morris, D. E.; Hanck, K. W.; DeArmond, M. K. *J. Am. Chem. Soc.* **1983**, *105*, 3032.
(14) Pierpont, C. G. *Coord. Chem. Rev.* **2001**, *216−217*, 99.
(15) Vlček, A., Jr. *Comments Inorg. Chem.* **1994**, *16*, 207.
(16) Adams, D. M.; Dei, A.; Rheingold, A. L.; Hendrickson, D. N. *J. Am. Chem. Soc.* **1993**, *115*, 8221.
(17) Neuwahl, F. V. R.; Righini, R.; Dei, A. *Chem. Phys. Lett.* **2002**, *352*, 408.
(18) Önfelt, B.; Lincoln, P.; Nordén, B.; Baskin, J. S.; Zewail, A. H. *Proc. Natl. Acad. Sci. U.S.A.* **2000**, *97*, 5708.
(19) Westmoreland, T. D.; Le Bozec, H.; Murray, R. W.; Meyer, T. J. *J. Am. Chem. Soc.* **1983**, *105*, 5952.
(20) Chen, P.; Danielson, E.; Meyer, T. J. *J. Phys. Chem.* **1988**, *92*, 3708.
(21) Chen, P.; Curry, M.; Meyer, T. J. *Inorg. Chem.* **1989**, *28*, 2271.
(22) Schoonover, J. R.; Chen, P.; Bates, W. D.; Dyer, R. B.; Meyer, T. J. *Inorg. Chem.* **1994**, *33*, 793.
(23) Liard, D. J.; Vlček, A., Jr. *Inorg. Chem.* **2000**, *39*, 485.
(24) Yeh, A. T.; Shank, C. V.; McCusker, J. K. *Science* **2000**, *289*, 935.
(25) Damrauer, N. H.; Cerullo, G.; Yeh, A.; Boussie, T. R.; Shank, C. V.; McCusker, J. K. *Science* **1997**, *275*, 54.
(26) Liard, D. J.; Kleverlaan, C. J.; Vlček, A., Jr. *Inorg. Chem.* **2003**, *42*, 7995.
(27) Ponce, A.; Gray, H. B.; Winkler, J. R. *J. Am. Chem. Soc.* **2000**, *122*, 8187.
(28) Vlček, A., Jr.; Farrell, I. R.; Liard, D. J.; Matousek, P.; Towrie, M.; Parker, A. W.; Grills, D. C.; George, M. W. *J. Chem. Soc., Dalton Trans.* **2002**, 701.
(29) Matousek, P.; Parker, A. W.; Taday, P. F.; Toner, W. T.; Towrie, M. *Opt. Commun.* **1996**, *127*, 307.
(30) Towrie, M.; Parker, A. W.; Shaikh, W.; Matousek, P. *Meas. Sci. Technol.* **1998**, *9*, 816.
(31) Matousek, P.; Towrie, M.; Stanley, A.; Parker, A. W. *Appl. Spectrosc.* **1999**, *53*, 1485.
(32) Matousek, P.; Towrie, M.; Ma, C.; Kwok, W. M.; Phillips, D.; Toner, W. T.; Parker, A. W. *J. Raman Spectrosc.* **2001**, *53*, 1485.
(33) Towrie, M.; Grills, D. C.; Dyer, J.; Weinstein, J. A.; Matousek, P.; Barton, R.; Bailey, P. D.; Subramaniam, N.; Kwok, W. M.; Ma, C. S.; Phillips, D.; Parker, A. W.; George, M. W. *Appl. Spectrosc.* **2003**, *57*, 367.
(34) Busby, M.; Matousek, P.; Towrie, M.; Vlček, A., Jr. Manuscript in preparation.
(35) Berger, S.; Klein, A.; Kaim, W.; Fiedler, J. *Inorg. Chem.* **1998**, *37*, 5664.
(36) Busby, M.; Liard, D. J.; Motevalli, M.; Toms, H.; Vlček, A., Jr. *Inorg. Chim. Acta* **2004**, *357*, 167.
(37) The value used was determined from the structure of $[Re(MQ^+)(CO)_3(bpy)]^{2+}$. The MQ^+ ligand in $[Re(MQ^+)(CO)_3(dmb)]^{2+}$ in a crystal is bent toward the dmb ligand, presumably due to electrostatic effects of the PF_6^- counterions shortening the electron-transfer distance to 7.596 Å. However, this tilt should disappear in the fluid solution where ILET actually occurs. Therefore, the value determined for $[Re(MQ^+)(CO)_3(bpy)]^{2+}$, where the Re−N−C−C−$N^+$−C axis of the Re−$MQ^+$ unit is straight, is more appropriate for the dmb complex.
(38) Mines, G. A.; Roberts, J. A.; Hupp, J. T. *Inorg. Chem.* **1992**, *31*, 125.
(39) Záliš, S.; Daniel, C.; Vlček, A., Jr. *J. Chem. Soc., Dalton Trans.* **1999**, 3081.
(40) Riddick, J. A.; Bunger, W. B.; Sakano, T. K. *Organic Solvents*; Wiley: New York, 1986.
(41) Kaplan, R.; Napper, A. M.; Waldeck, D. H.; Zimmt, M. B. *J. Phys. Chem. A* **2002**, *106*, 1917.
(42) Omberg, K. M.; Chen, P.; Meyer, T. J. In *Electron Transfer—From Isolated Molecules to Biomolecules. Part II. Advances in Chemical Physics*; Jortner, J., Bixon, M., Eds.; J. Wiley & Sons: New York, 1999; Vol. 106, p 553.
(43) Dattelbaum, D. M.; Meyer, T. J. *J. Phys. Chem. A* **2002**, *106*, 4519.
(44) Worl, L. A.; Duesing, R.; Chen, P.; Della Ciana, L.; Meyer, T. J. *J. Chem. Soc., Dalton Trans.* **1991**, 849.
(45) Dattelbaum, D. M.; Omberg, K. M.; Schoonover, J. R.; Martin, R. L.; Meyer, T. J. *Inorg. Chem.* **2002**, *41*, 6071.

(46) Yaws, C. L. *Chemical Properties Handbook*; McGraw-Hill: New York, 1999.
(47) *CRC Handbook of Chemistry and Physics*; CRC Press: Boca Raton, FL, 2002.
(48) Horng, M. L.; Dahl, K.; Jones II, G.; Maroncelli, M. *Chem. Phys. Lett.* **1999**, *315*, 363.
(49) Kahlow, M. A.; Kang, T. J.; Barbara, P. F. *J. Chem. Phys.* **1988**, *88*, 2372.
(50) Jarzeba, W.; Walker, G. C.; Johnson, A. E.; Barbara, P. F. *Chem. Phys.* **1991**, *152*, 57.
(51) Shirota, H.; Pal, H.; Tominaga, K.; Yoshihara, K. *J. Phys. Chem.* **1996**, *100*, 14575.
(52) Horng, M. L.; Gardecki, J. A.; Papazyan, A.; Maroncelli, M. *J. Phys. Chem.* **1995**, *99*, 17311.
(53) Bates, W. D.; Chen, P.; Bignozzi, C. A.; Schoonover, J. R.; Meyer, T. J. *Inorg. Chem.* **1995**, *34*, 6215.
(54) Liard, D. J.; Towrie, M.; Busby, M.; Matousek, P.; Vlček, A., Jr. *J. Phys. Chem. A* **2004**, in press.
(55) Treffert-Ziemelis, S. M.; Golus, J.; Strommen, D. P.; Kincaid, J. R. *Inorg. Chem.* **1993**, *32*, 3890.
(56) Mallick, P. K.; Strommen, D. P.; Kincaid, J. R. *J. Am. Chem. Soc.* **1990**, *112*, 1686.
(57) Mallick, P. K.; Danzer, G. D.; Strommen, D. P.; Kincaid, J. R. *J. Phys. Chem.* **1988**, *92*, 5628.
(58) Ghoshal, S.; Lu, T.; Feng, Q.; Cotton, T. M. *Spectrochim. Acta* **1988**, *44A*, 651.
(59) Poizat, O.; Buntinx, G.; Ventura, M.; Lautié, M. F. *J. Phys. Chem.* **1991**, *95*, 1245.
(60) Feng, Q.; Cotton, T. M. *J. Phys. Chem.* **1986**, *90*, 983.
(61) Záliš, S.; Farrell, I. R.; Vlček, A., Jr. *J. Am. Chem. Soc.* **2003**, *125*, 4580.
(62) Asher, S. A.; Murtaugh, J. *J. Am. Chem. Soc.* **1983**, *105*, 7244.
(63) Hamm, P.; Ohline, S. M.; Zinth, W. *J. Chem. Phys.* **1997**, *106*, 519.
(64) Nakabayashi, T.; Kamo, S.; Sakuragi, H.; Nishi, N. *J. Phys. Chem. A* **2001**, *105*, 8605.
(65) Hirata, Y.; Okada, T. *Chem. Phys. Lett.* **1991**, *187*, 203.
(66) Iwata, K.; Hamaguchi, H. *J. Mol. Liq.* **1995**, *65/66*, 417.
(67) Iwata, K.; Hamaguchi, H. *J. Phys. Chem. A* **1997**, *101*, 632.
(68) Hamaguchi, H.; Iwata, K. *Bull. Chem. Soc. Jpn.* **2002**, *75*, 883.
(69) Michelsen, H.; Kleboe, P.; Hagen, G.; Stroyer-Hansen, T. *Acta Chem. Scand.* **1972**, *26*, 1576.
(70) Glyn, P.; George, M. W.; Hodges, P. M.; Turner, J. J. *J. Chem. Soc., Chem. Commun.* **1989**, 1655.
(71) George, M. W.; Johnson, F. P. A.; Westwell, J. R.; Hodges, P. M.; Turner, J. J. *J. Chem. Soc., Dalton Trans.* **1993**, 2977.
(72) Gamelin, D. R.; George, M. W.; Glyn, P.; Grevels, F.-W.; Johnson, F. P. A.; Klotzbucher, W.; Morrison, S. L.; Russell, G.; Schaffner, K.; Turner, J. J. *Inorg. Chem.* **1994**, *33*, 3246.
(73) Turner, J. J. *Coord. Chem. Rev.* **2002**, *230*, 212.
(74) Asbury, J. B.; Wang, Y.; Lian, T. *Bull. Chem. Soc. Jpn.* **2002**, *75*, 973.
(75) Jortner, J.; Bixon, M. *J. Chem. Phys.* **1988**, *88*, 167.
(76) Bixon, M.; Jortner, J. *Chem. Phys.* **1993**, *176*, 467.
(77) Sumi, H.; Marcus, R. A. *J. Chem. Phys.* **1986**, *84*, 4894.
(78) Bagchi, B.; Gayathri, N. In *Electron Transfer—From Isolated Molecules to Biomolecules. Part II. Advances in Chemical Physics*; Jortner, J., Bixon, M., Eds.; J. Wiley and Sons, Inc.: New York, 1999; Vol. 107, p 1.
(79) Yoshihara, K. In *Electron Transfer—From Isolated Molecules to Biomolecules. Part II. Advances in Chemical Physics*; Jortner, J., Bixon, M., Eds.; J. Wiley and Sons, Inc.: New York, 1999; Vol. 107, p 371.
(80) Newton, M. D. In *Electron Transfer in Chemistry*; Balzani, V., Ed.; Wiley-VCH: Weinheim, Germany, 2001; Vol. 1, p 3.
(81) Tominaga, K.; Kliner, D. A. V.; Johnson, A. E.; Levinger, N. E.; Barbara, P. F. *J. Chem. Phys.* **1993**, *98*, 1228.
(82) Xu, Q.-H.; Scholes, G. D.; Yang, M.; Fleming, G. R. *J. Phys. Chem. A* **1999**, *103*, 10348.
(83) Collin, J.-P.; Harriman, A.; Heitz, V.; Odobel, F.; Sauvage, J.-P. *J. Am. Chem. Soc.* **1994**, *116*, 5679.
(84) Katz, N. E.; Mecklenburg, S. L.; Graff, D. K.; Chen, P.; Meyer, T. J. *J. Phys. Chem.* **1994**, *98*, 8959.